Analytical Model for Determination of the Unipolar Ionic Saturation Current During Positive Corona Discharge for Geometries Comprising Cylindrical Emitter Electrodes

Emmanouil D. Fylladitakis
Brunel University London
Department of Electronic & Computer Engineering
Uxbridge, Middlesex, UB8 3PH, London, UK

Antonios X. Moronis
Technological Educational Institute (TEI) of Athens
Department of Energy Technology Engineering
Aegaleo, 12210, Athens, Greece

and **Michael Theodoridis**
Brunel University London
Department of Electronic & Computer Engineering
Uxbridge, Middlesex, UB8 3PH, London, UK

ABSTRACT

This paper presents an analytical model for the assessment of the unipolar corona saturation current limit for positive corona discharge in air, based on the determination of the field line lengths and trajectories. The model is applicable to emitter electrodes with a cylindrical surface facing a plane or an identical cylindrical collector electrode, if their spatial characteristics, the ion mobility of the surrounding medium and the applied voltage are known. Experimental investigation is performed to compare the results of the unipolar corona saturation current limit from the proposed model to the actual corona current flow in an experimental setup that comprises cylindrical emitters of various radii, facing a plane electrode. Both the total current amplitude and the current density distribution over the collecting electrode's surface have been examined.

Index Terms - **Corona discharge, electrohydrodynamics (EHD), unipolar corona saturation current, ionic Wind.**

1 INTRODUCTION

THE phenomenon of corona discharge is being used in numerous electrostatic processes [1]. Application examples include propulsion methods [2, 3], surface cooling [4], pollution control [5], cooling augmentation [6], and even agricultural applications [7]. Corona discharge initiates when adequate voltage potential is applied to an electrode with a sufficiently sharp edge or a small curvature radius, generating a strong electric field that ionizes some of the surrounding medium molecules (usually atmospheric air). The charged molecules then move towards the collector electrode. This charged particle flow effect is the hallmark of corona discharge in gases [8]. Generally, a corona discharge is characterized by two regions; a small region very close to the surface of the emitter electrode, the ionization region, and the drift region, where the ionized gas molecules are forced towards the collector electrode [9]. The complete mechanism behind the corona discharge becomes quite complicated when the phenomena taking place inside the ionization region need to be taken into account [10], but the overall system can be dramatically simplified by neglecting the effects inside the ionization region - an approach generally suitable for the assessment of macroscopic parameters. Specifically, the macroscopic solution of this complex phenomenon can be greatly simplified by assuming that only unipolar ions are created and drifting with constant mobility in the gas. Unipolar flow is the dominant type of flow with low current coronas, in significantly inhomogeneous electric fields, where the ionization region is confined very close to the emitter electrode and most of the drift region is filled with a low electric field [9].

The determination of the electric field and ionic current distribution is very useful in order to fully understand the phenomenon and, in extend, the mechanisms behind the applications making use of corona discharges. Today, there are several applications in which wire-cylinder electrode

Manuscript received on 9 December 2015, in final form 11 November 2016, accepted 5 December 2016. Corresponding author: E. D. Fylladitakis.

configurations are being used, such as ozone generators [11] and aerodynamics [12], while they also might find future use in other applications as well, where other electrode configurations are already being used, such as electrostatic precipitators [13], fluid accelerators [14-16] and electrospraying [17, 18].

In this paper, mathematical solutions are given for the determination of the saturated unipolar ionic current and its distribution over the collecting electrode's surface. The cylinder-plane and twin cylinder-cylinder electrode configurations have been studied. The mathematical model is also being experimentally verified. It must be noted that only positive coronas have been examined due to the fact that they are more stable and efficient for most applications [19, 20].

2 METHODOLOGY

Assuming parallel cylindrical electrode configurations with infinite length and symmetrically connected sources/sinks, the analytical model of the field lines can be worked out in two dimensions, due to the existing longitudinal symmetry. When two cylindrical conductors are at the same potential with reference to predominantly earth potential far away from the conductors, a "bundle conductors" configuration is formed, where the field distribution can be calculated by assuming only two line charges running in parallel and eccentrically placed within the conductors, which is a method extensively applied in high voltage transmission lines [21-24]. The electric field is depending only on the distance perpendicular to the conductors, thus remaining unchanged along the longitudinal dimension. Therefore, the formation of equipotential lines in any case is a set of circles, with their center always on the *X* axis [25]. Thus, considering a plane vertical to the electrodes axis, the field lines can be described as circular arcs, vertically emerging from, or impinging to the electrode surfaces, with direction from the emitter (positive electrode) towards the collector (negative or grounded electrode). These lines can be defined using circle equations with centers placed on the *Y*-axis, as shown in Figure 1.

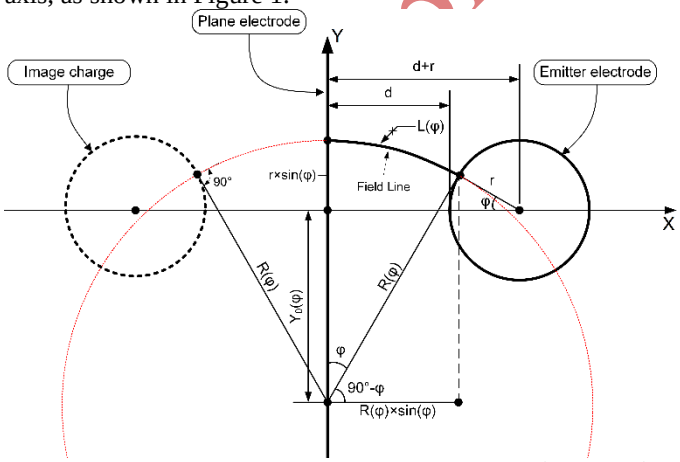

Figure 1. Parallel cylinders/Cylinder to plane electrode configuration, field lines formation.

On the other hand, each field line equation should be also depending on its emergence angle φ. In the case of a cylinder to plane configuration, a similar distribution exists, since the plane can be replaced equivalently by a second cylindrical electrode acting as "image charge", at the opposite side of the plane, at equal distance [21, 26]. In this case the model of the field lines remains the basically same, except the fact that now the total length of the field lines is halved.

With reference to the geometry of Figure 1, we need first to define the radius $R(\varphi)$ and the center position $Y_0(\varphi)$ of each field line equation. Then we could easily estimate the corresponding length $L(\varphi)$ of each field line, considering the fact that the field lines are always perpendicular to the electrode surfaces.

3 NUMERICAL MODEL

3.1 CYLINDER-PLANE CONFIGURATION

According to Figure 1, we have that:

$$Y_0(\varphi) = R(\varphi)\cos(\varphi) - r\sin(\varphi) \tag{1}$$

The radius R(φ) of the circle defining each field line is given by:

$$R(\varphi) = \frac{x_0 - r\cos(\varphi)}{\sin(\varphi)} \tag{2}$$

where $x_0 = d + r$, with d representing the cylinder-plane distance and r representing the radius of the cylinder.

By combining equation (1) and (2) and rearranging, we finally get the position of the circle's center on the Y axis:

$$Y_0(\varphi) = x_0\cot(\varphi) - r\,csc\,(\varphi) \tag{3}$$

Therefore, for any given field line emerging with angle φ, the position of the defining circle's center on the *Y* axis and its radius are known.

For a cylinder-plane geometry the total field line length is in fact the full arc length covered by angle φ as follows:

$$L(\varphi) = \varphi\, R(\varphi) = \frac{\varphi\,(x_0 - r\cos(\varphi))}{\sin(\varphi)} = \frac{\varphi\,(d + r - r\cos(\varphi))}{\sin(\varphi)} \tag{4}$$

In the case of two parallel cylindrical conductors the total field line length should be two times the corresponding field line length for the case of a cylindrical conductor parallel to a plane, at a given angle φ.

Figure 2 illustrates an example of the estimated field lines in a cylinder-plane electrode configuration at distance d = 5 cm, for V = 1 kV and r = 0.5 cm, at different angles φ, ranging from 0 to 90 degrees, in 30 degree steps.

It is known that the saturation current can be expressed in relation to the length of the field line [9, 10, 27]. The unipolar saturation current density limit j_s across any field line of length L crossing a gap of voltage V, is given by:

$$j_s = \mu\,\varepsilon_0\frac{V^2}{L^3} \tag{5}$$

where μ is the average ion mobility of the fluid in the gap and ε_0 is the vacuum permittivity. The average ion mobility in air is usually considered to be (1.8 - 2.2) × 10^{-4} $m^2/V{\times}s$, with

references indicating that it can be as low as 1.3×10^{-4} m^2/V×s and as high as 2.6×10^{-4} m^2/V×s [28-31].

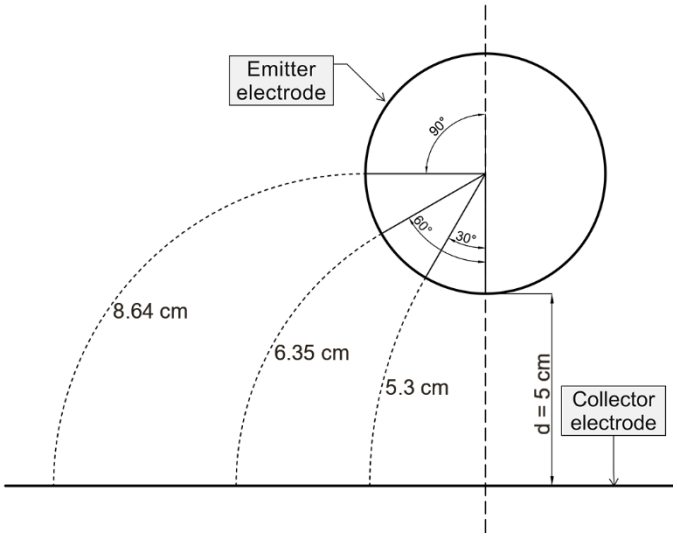

Figure 2. Field lines formation in a cylinder-plane electrode configuration, for V = 1 kV, d = 5 cm and r = 0.5 cm in 30° steps, up to 90°.

For a cylinder to plane configuration, the insertion of equation (4) into equation (5) results to:

$$j_s(\varphi) = \mu\, \varepsilon_0\, V^2 \frac{\sin^3(\varphi)}{\varphi^3 (d + r - r\cos(\varphi))^3} \left(\frac{A}{m^2}\right) \tag{6}$$

where φ is the emergence angle of the field lines, as illustrated in Figure 1.

With reference to Figure 3, if we consider an elementary strip on the plane, at distance $\Delta(\varphi)$ from the vertical projection of the cylindrical conductor axis, $d\Delta(\varphi)$ wide, then the strip's contribution to the total saturation current is:

$$dI_{s\,c-p}(\varphi) = d\Delta(\varphi) \times j_s(\varphi) \left(\frac{A}{m}\right) \tag{7}$$

where $\Delta(\varphi)$ can be calculated by using equations (1) and (2) as:

$$\Delta(\varphi) = R(\varphi) - Y_0(\varphi) = (d + 2r)\frac{(1 - cos(\varphi))}{\sin(\varphi)} \tag{8}$$

Differentiating equation (8) with respect to angle φ we get that:

$$d\Delta(\varphi) = \frac{d + 2r}{1 + \cos(\varphi)} d\varphi \left(\frac{A}{m}\right) \tag{9}$$

Finally, after substituting equations (6) and (9) in equation (7), the total saturation current limit $I_{s\ c\text{-}p,}$ flowing per unit length of the cylindrical emitter can then be estimated by integrating
$dI_{s\ c\text{-}p}$ over the cylinder's surface:

$$I_{s\,c-p} = 2\int_0^{\pi} dI_{s\,c-p}(\varphi)$$
$$= 2\,\mu\,\varepsilon_0\,V^2 \int_0^{\pi} \frac{d + 2r}{1 + \cos(\varphi)} \frac{\sin^3(\varphi)}{\varphi^3 (d + r - r\cos(\varphi))^3}\, d\varphi \tag{10}$$

The unipolar saturation current limit I_s represents the maximum possible current flow between the electrodes, assuming that the current flow is kept entirely unipolar, i.e. during normal corona flow. However, by approaching breakdown regime it is possible for the actual current to exceed the saturation current limit due to bipolar conduction phenomena or streamer breakout [9].

It should be noted that, although the collecting plane electrode is generally considered to have infinite dimensions in the analysis presented above, Equation (10) shows that the total current flow is actually confined within distance $\Delta(\pi)$ (given by equation (8)) to either side of the emitting cylindrical electrode (since the field lines extend up to this distance at most). Furthermore, it should also be noted that the proposed model has certain limitations. Because the model relies on the longitudinal symmetry of the arrangement, the presence of substantial space charges or an unevenly distributed potential across the electrodes can disrupt the formation of the electric field, deforming the electric field lines (e.g. shifting them from circular to elliptical arcs) and, thus, reducing its accuracy. A similar phenomenon occurs at the ends of the arrangements, where the longitudinal symmetry ceases to exist and the electric field is deformed. However, as long as the arrangement's total length is substantially greater than the electrode gap d, the contribution of the deformed field lines near the end of the arrangement to the total current could be considered insignificant.

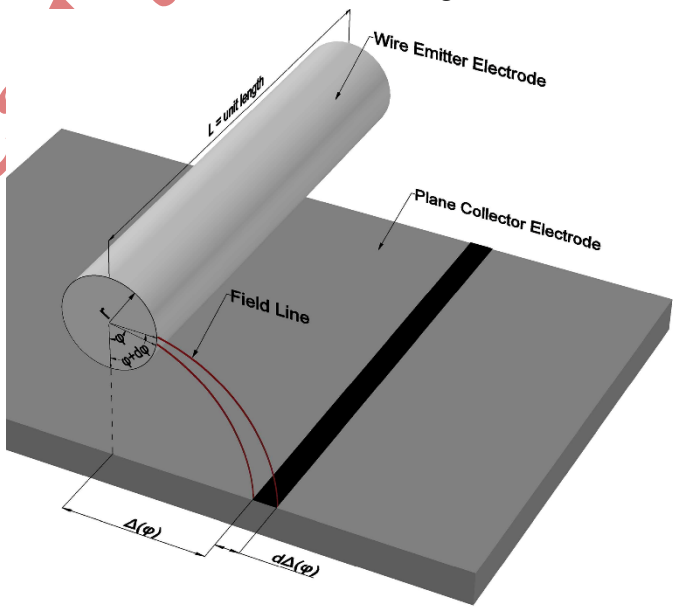

Figure 3. Indicative schematic, (equation (8)).

For applications that rely on corona discharge, the above solution can be simplified, assuming that $d \gg r$. In that case, Equation (6) becomes:

$$j_s(\varphi) = \mu\, \varepsilon_0\, V^2 \frac{\sin^3(\varphi)}{\varphi^3 d^3} = \left(\frac{\mu\, \varepsilon_0\, V^2}{d^3}\right)\left(\frac{\sin(\varphi)}{\varphi}\right)^3 \left(\frac{A}{m^2}\right) \tag{11}$$

However, it is known that the maximum current density across the gap is [9]:

$$j_0 = \frac{\mu\, \varepsilon_0\, V^2}{d^3} \left(\frac{A}{m^2}\right) \tag{12}$$

The combination of equations (11) and (12) result to equation (13), which suggests that the current density $j_s(\varphi)$ is altering according to Warburg's law.

$$j_s(\varphi) = j_0 \left[\frac{\sin(\varphi)}{\varphi}\right]^3 \left(\frac{A}{m^2}\right) \quad (13)$$

Furthermore, the assumption that $d \gg r$ also simplifies Equation (9):

$$d\Delta(\varphi) = \frac{d}{1+\cos(\varphi)} d\varphi \left(\frac{A}{m}\right) \quad (14)$$

Therefore, equation (10) can be greatly simplified by numerically evaluating the integrating part and becomes:

$$I_{s\,c-p} = \frac{2\,\mu\,\varepsilon_0 V^2}{d^2} \int_0^{\pi} \frac{\sin^3(\varphi)}{\varphi^3[1+\cos(\varphi)]}\, d\varphi = \frac{1.62\,\mu\,\varepsilon_0 V^2}{d^2} \left(\frac{A}{m}\right) \quad (15)$$

Based on the same methodology, the solutions for more electrode configurations can be easily derived as well, as discussed in the next session.

3.2 TWIN CYLINDER-CYLINDER CONFIGURATIONS

Based on the same methodology, the solutions for more electrode configurations can be easily derived as well.

For a twin cylinder-cylinder configuration, as illustrated in Figure 4, the field lines length $L(\varphi)$ given by equation (4), should be multiplied by 2 (length is doubled) while the maximum unipolar saturation current limit per unit length is equal to:

$$I_{s\,c-c} = 2\int_0^{\pi} dI_S(\varphi) = 2\int_0^{\pi} r \times j_s(\varphi)\, d\varphi \left(\frac{A}{m}\right) \quad (16)$$

Consequently, the total unipolar saturation current of a twin cylinder-cylinder electrode configuration is:

$$I_{s\,c-c} = 2\,\mu\,\varepsilon_0\,V^2 \int_0^{\pi} r\, \frac{\sin^3(\varphi)}{(2\varphi)^3(d+r-r\cos(\varphi))^3}\, d\varphi \left(\frac{A}{m}\right) \quad (17)$$

Equation (17) can also be simplified by assuming that $d \gg r$ and then numerically evaluating the integration. In that case, we have that:

$$I_{s\,c-c} = \frac{\mu\,\varepsilon_0\,V^2 r}{4d^3} \int_0^{\pi} \left[\frac{sin(\varphi)}{\varphi}\right]^3 d\varphi = \frac{0.2974 * \mu\,\varepsilon_0\,V^2 r}{d^3} \left(\frac{A}{m}\right) \quad (18)$$

The previously described analysis could also be applied in the case of spherical electrodes, although there is a major difference in the geometry, since the electrodes do not exhibit a longitudinal symmetry anymore. However, the field lines could yet be described by circular arcs, vertically emerging from the spherical emitter's surface and then impinging vertically on the surface of the collector whichever type that is (plane or spherical). So, in spherical geometries, the results are expressed in terms of the total saturation current as a whole, rather than per unit length as in the previous sections.

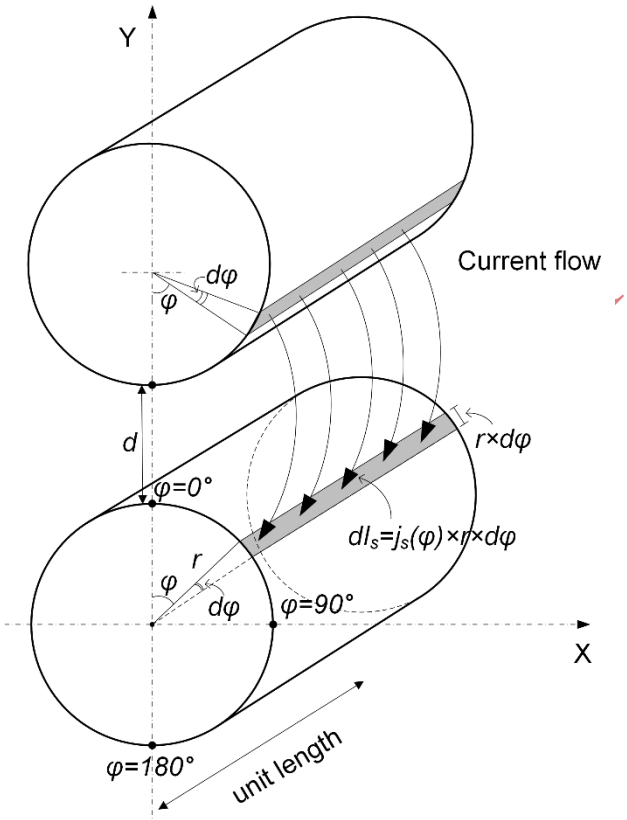

Figure 4. Indicative schematic of the field lines in a cylinder-cylinder configuration.

4 EXPERIMENTAL CONFIGURATION

In order to investigate the validity of the developed mathematical models, measurements have been carried out in order to specify the total corona current flowing between the electrodes at different voltage levels before breakdown occurs, in a cylinder-plane configuration. Also the current density over the plane has been measured as a function of distance from the cylinder's axis vertical projection on the plane. On that purpose, Ni-Cr wires of different diameters were used as emitters above a flat aluminum plate (collector). A simplified schematic of the experimental setup is given in Figure 5.

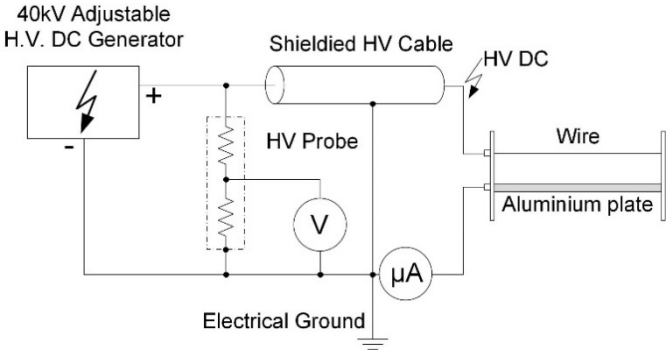

Figure 5. Experimental setup.

The required high voltage was supplied by an adjustable high voltage power source (Matsusada Precision W Series). A voltmeter combined with a Coline HV40B 40 kV 1000:1 high voltage probe were used for measuring the DC high voltage

applied to the emitter electrode, with an accuracy of 1%. Current readings (corona current) have been acquired by a high precision Thurlby 1503 ammeter with 10 nA sensitivity. All the experiments were performed in atmospheric air, with temperature ranging from 25 to 27 °C, and relative humidity between 45 and 52 %. Also, in order to specify the current density distribution over the plate, a thin conductive strip was used, electrically isolated from the remaining part of the plate. As the thickness of the strip was less than 30 μm, which is very small compared to the gap *d*, its effect on the overall electric field distribution was considered to be negligible. The unipolar saturation current corresponding to that strip is defined by Equation (10), multiplying by the strip's length *L*:

$$I_s = \mu\,\varepsilon_0\,V^2 L \int_{\varphi_1}^{\varphi_2} \frac{d+2r}{1+\cos(\varphi)} \times \frac{\sin^3(\varphi)}{\varphi^3 (d+r-r\cos(\varphi))^3}\, d\varphi \quad A \tag{19}$$

where *L* is the length of the strip and φ_1, φ_2 are the emergence angles of the field lines landing at the strip edges over its width. The strip was 2.5 mm wide.

As the current going through the strip is very small, a resistor was connected between the strip and the electrical ground, with a precision Mastech MS8218 voltmeter measuring the voltage drop. Figure 6 displays a graphical representation of the experimental setup.

5 RESULTS AND DISCUSSION

5.1 FULL PLANE SATURATION CURRENT LIMIT

As the value of the ion mobility μ in air varies in bibliography, we demonstrate the saturation current density limit, in a cylinder-plane geometry, as an area formed by the results calculated with an ion mobility between 1.8×10^{-4} m^2/V×s and 2.2×10^{-4} m^2/V×s, which are the most widely used values for air [28, 29]. The saturation current limit shown in Figures 7, 8, 9, 10, 11, 14 and 15 is calculated via Equation (19). As it can be seen in Figure 7 and Figure 8, the corona current tends to approach and or slightly exceed the saturation current limit near the breakdown point of the geometry. This is the natural development of the phenomenon, as the ionic drift region outside the ionization region acts as an impedance that gives the corona discharge its characteristic intrinsic stability [29]. In electrode configurations with a very small electrode gap *d*, the saturation current limit tends to be considerably higher than the actual corona current (Figure 9). On the contrary, Figure 10 depicts that formations with considerable gaps but very small electrode radius can result to a corona current higher than the unipolar saturation current limit.

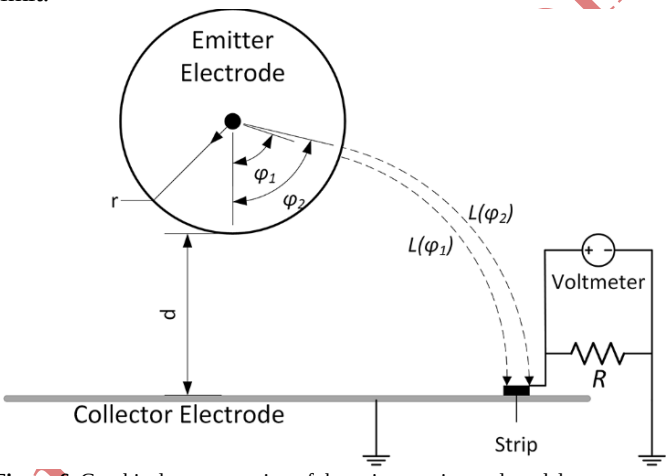

Figure 6. Graphical representation of the strip experimental model.

Corona currents are strongly dependent on the electric field strength [32, 33]. Therefore, higher electric field strengths are expected to generate higher corona currents. However, in the case of Figure 9, the high electric field strength and relatively small ionic drift region in the space between the electrodes makes corona discharge lose its stability and results to a breakdown long before saturation can be achieved. This effect becomes more apparent as the radius of the emitter increases, which results to higher saturation current limits due to the large theoretical drift region formed by the long field lines, yet the short space and very strong electric field within the space directly between the electrodes (φ = 0°) brings the geometry to breakdown far before high corona currents may be realized.

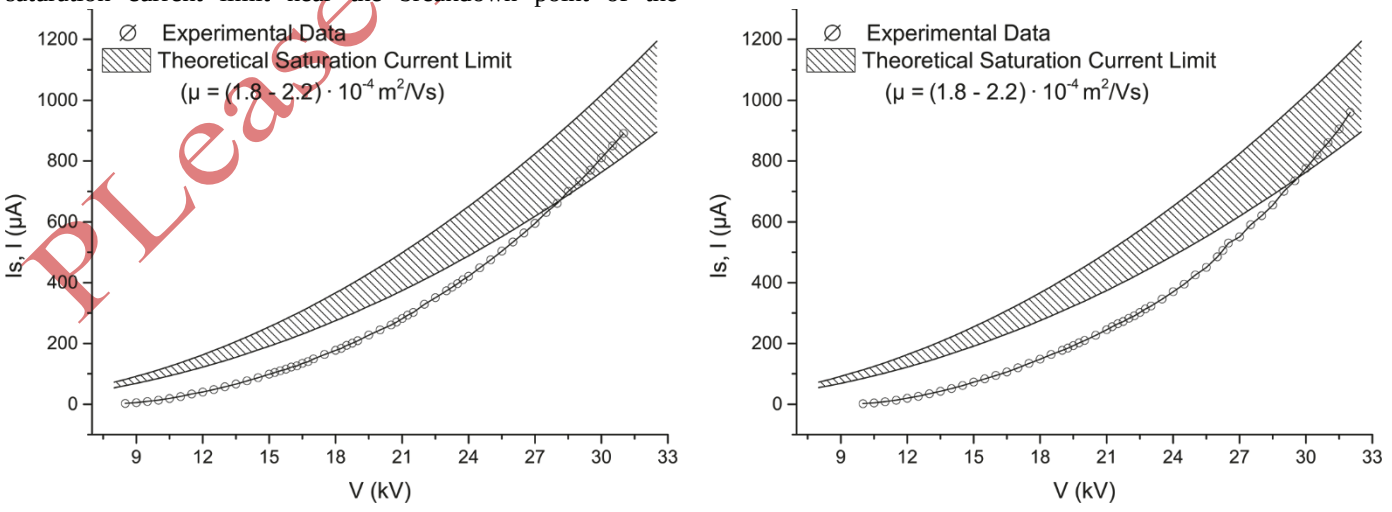

Figure 7. Correlation between the corona current I and the calculated saturation current limit I_S in a cylinder-plane geometry, for d = 3 cm, r = 100 μm (left) and d = 3 cm, r = 140 μm (right).

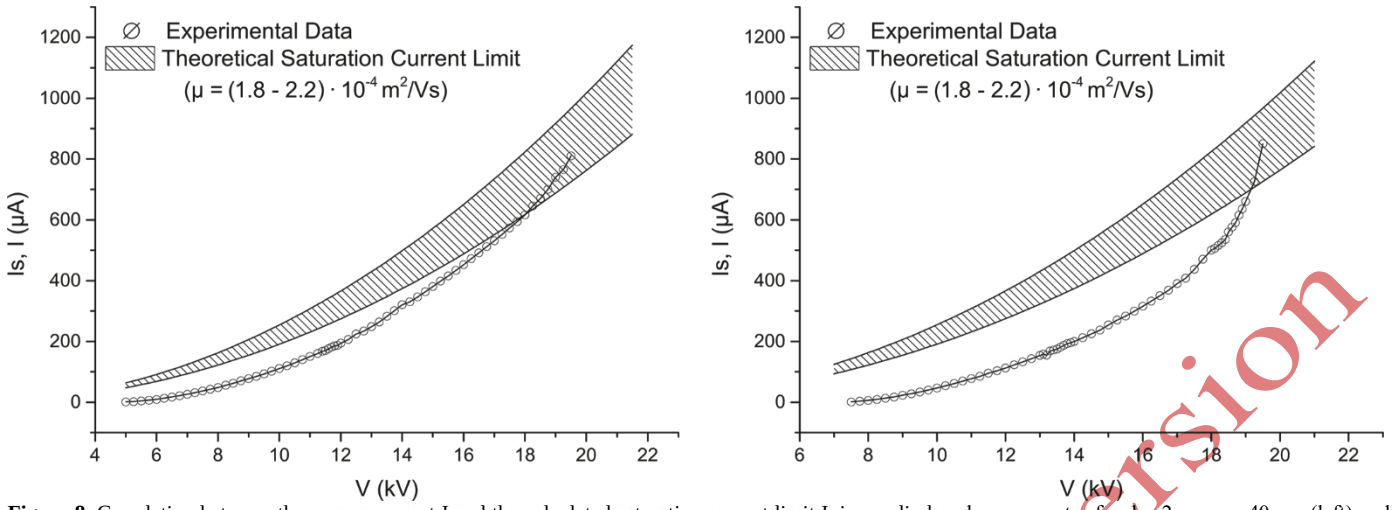

Figure 8. Correlation between the corona current I and the calculated saturation current limit I_S in a cylinder-plane geometry for d = 2 cm, r = 40 μm (left) and d = 2 cm, r = 100 μm (right).

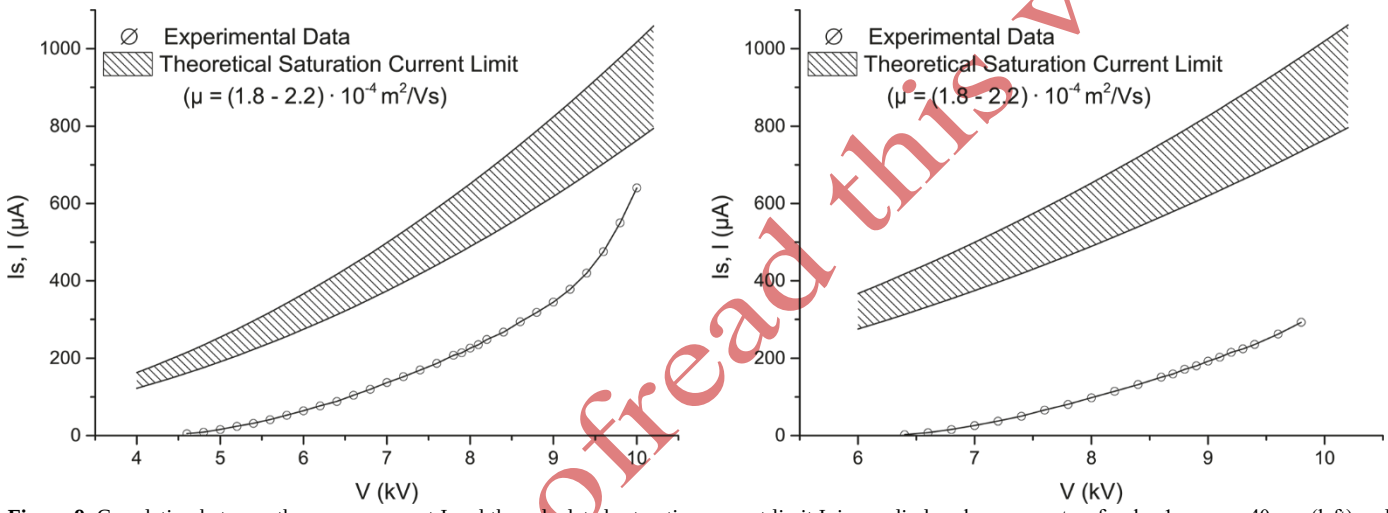

Figure 9. Correlation between the corona current I and the calculated saturation current limit I_S in a cylinder-plane geometry, for d = 1 cm, r = 40 μm (left) and d = 1 cm, r = 100 μm (right).

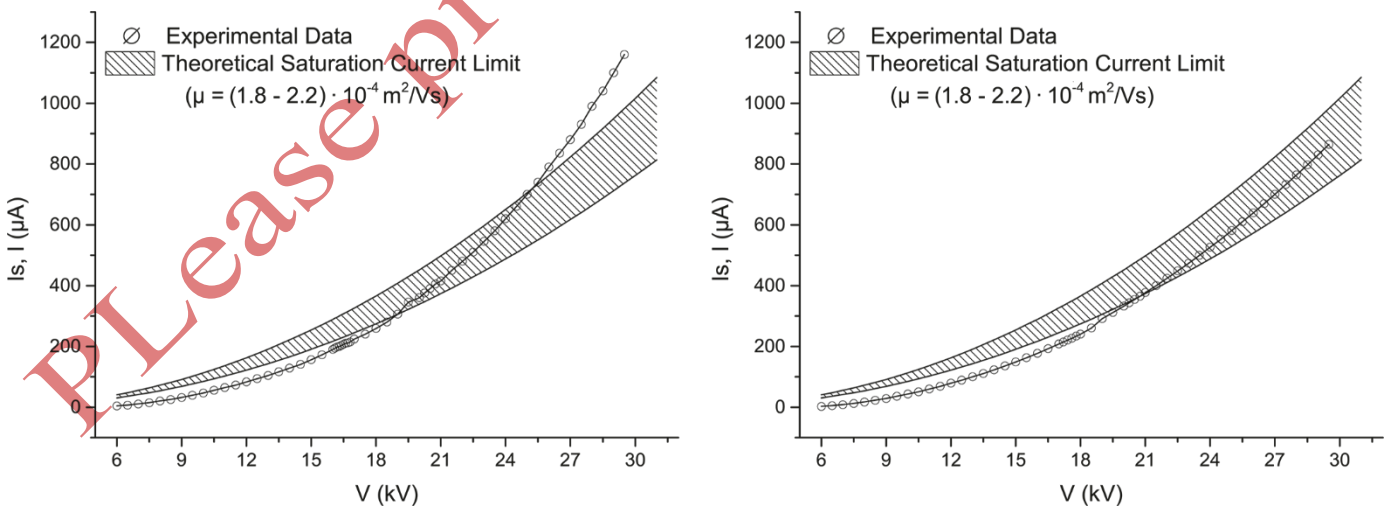

Figure 10. Correlation between the corona current I and the calculated saturation current limit I_S in a cylinder-plane geometry, for d = 3 cm, r = 30 μm (left) and d = 3 cm, r = 40 μm (right).

On the other hand, larger gaps and very small electrode radii are expected to generate high corona currents. Assisted by the high impedance of the now expanded drift region between the electrodes, the emitter's voltage can be increased while maintaining fair corona current flow stability. In this case, the strong electric field and the high field inhomogeneity in the space between the electrodes, may result to ions of higher mobility, as well as to the

formation of bipolar conduction phenomena (e.g. streamers), producing corona currents higher than the anticipated unipolar conduction limit [9, 32, 34, 35].

5.2 SATURATION CURRENT DENSITY DISTRIBUTION

In this section we examine the corona current flow through narrow (2.5 mm) sections of a plane collector. Due to the very small currents that need to be measured, a resistor is added between the strip and the electrical ground. By measuring the voltage drop across the resistor, the exact current can be calculated.

Generally, and as depicted in Figure 11, the corona current is greater for a given distance *d* and voltage *V* as the radius of the emitter decreases. This is in good agreement with the known theory of corona discharge, as the stronger and more inhomogeneous electric field generates a greater current flow. Still, the relatively small radii difference of the emitter compared to the distance d results to field lines of about equal length. As a result, the normalized contribution of each field line for a changing *r* is nearly identical (Figure 12). Changes of the electrode gap d have a significantly greater effect on the contribution of the field lines in relation to the emission angle φ, as the length of the field lines increases significantly.

As it is shown in Figure 12, the longer the electrode gap is, the greater the contribution of small emission angles becomes. On the other hand, smaller electrode gaps reduce the contribution of large emission angles. Figure 13 displays the experimentally measured corona current on the strip positioned across the plane electrode for different voltages *V*.

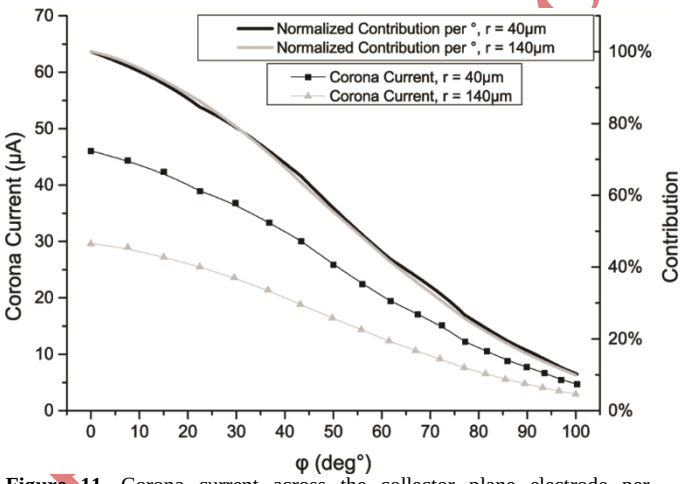

Figure 11. Corona current across the collector plane electrode per emission angle φ for d = 3 cm, V = 25 kV.

According to the proposed theoretical model, it is expected that field lines emanating from smaller emission angles will have a greater contribution towards the total corona current. The shorter ion flight path through the high impedance drift region and the stronger electric field between the electrodes, makes it easier for higher mobility ions to appear and favours the formation of bipolar transport phenomena. This is in good agreement with the developed mathematical model and the experimental results. Figure 14 indicates that the majority of the total current (≈90%) is contributed by the field lines with an emission angle up to 100° and that the current distribution is virtually unaffected by the voltage. Figure 14 seems to resemble Warburg's distribution where current density is reduced with $cos(\varphi)^m$, which has been experimentally observed for various geometries [36, 37].

In comparison to the theoretical unipolar saturation current limit of the geometry, it would appear that the actual contribution to the total corona current leans towards the shorter field lines. As it can be seen in Figure 15, small emission angles φ contribute the most to the overall corona current but may also override the saturation current limit significantly before breakdown occurs, while large emission angles may not exceed it at all. This may be attributed to the fact that the field lines emanating from smaller emission angles are shorter and travel through a drift region where a stronger electric field is present, while field lines emanating from higher emission angles travel

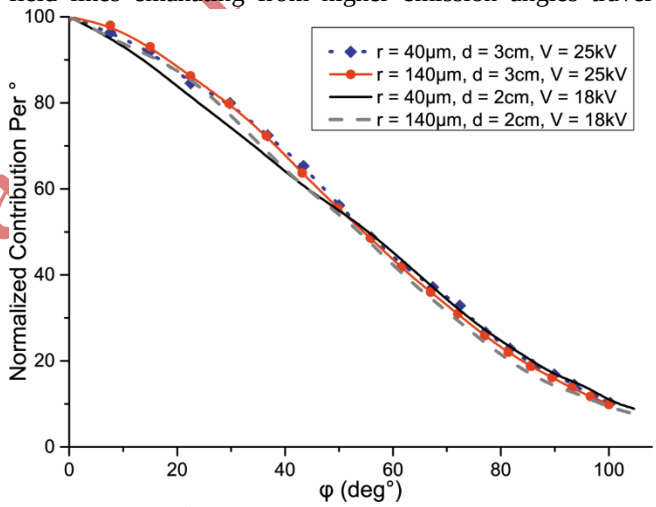

Figure 12. Fitted field line corona current contribution reduction in relation to the emission angle.

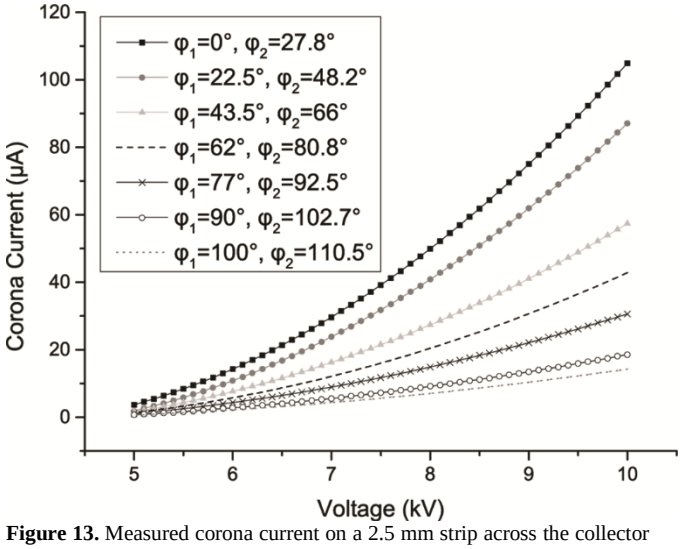

Figure 13. Measured corona current on a 2.5 mm strip across the collector plane electrode, in a cylinder-plane configuration, for d = 3 cm, r = 140 μm.

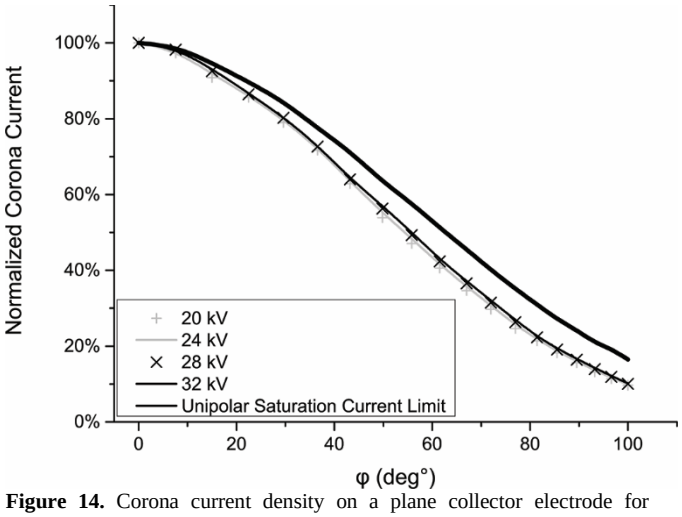

Figure 14. Corona current density on a plane collector electrode for varying angle φ, with d = 3 cm, r = 140 μm.

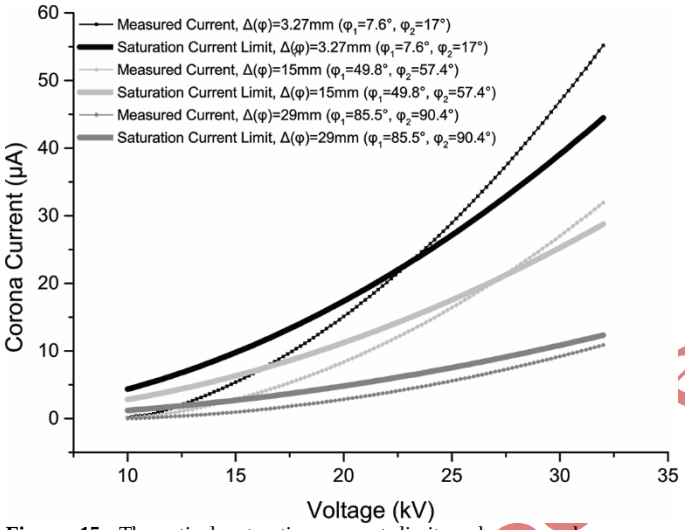

Figure 15. Theoretical saturation current limit and measured corona current at the strip for three different positions of the strip on a plane collector electrode (2.5 mm strip, d = 3 cm, r = 140 μm, $\mu = 1.8 \times 10^{-4}$ m^2/V×s).

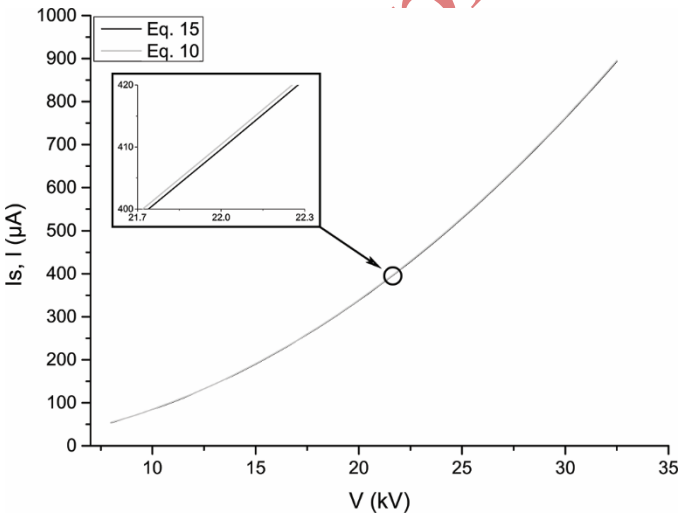

Figure 16. Comparison between the analytical model (equation (10)) and the simplified model (equation (15)). (d = 3 cm, r = 140 μm, $\mu = 1.8 \times 10^{-4}$ m^2/V×s).

through a longer drift region with greater overall impedance. The high currents at smaller emission angles at high voltages differences indicate the breakout of bipolar conduction phenomena in the space between the electrodes.

Finally, to verify the accuracy of the simplified equation (15), calculations were performed to compare its results to those of equation (10). The differences, as it can be seen from the indicative Figure 16, were miniscule, verifying that the simplified model is applicable.

6 Conclusions

The work presented in this paper introduces an analytical solution for the assessment of the unipolar saturation current limit in cylinder-plane and twin cylinder-cylinder electrode configurations. With the proposed model, which is based on the mathematical analysis of the field lines, an exact solution is presented, giving the precise length of each field line crossing the gap between a cylindrical emitter parallel to a plane collector or parallel to an identical cylindrical collector. Then, the unipolar saturation current amplitude, as well as the corresponding saturation current density variation across the surface of the collecting electrode, was analytically calculated for different geometrical parameters of the electrodes.

The proposed mathematical model was experimentally tested in a cylinder - plane configuration by using emitters of varying radius and varying gaps. Both the total discharge current and the distribution of the corona discharge current density across the plane have been investigated. The experimental results were compared to the calculated values from the proposed mathematical model. According to these results, the corona discharge current on the collecting electrode is following a distribution where the bulk of the corona discharge current ejects from the lower half of the emitting electrode's surface, which is closer to the collector.

REFERENCES

[1] A. D. Moore, *Electrostatics and its applications*, Wiley, 1973.

[2] D. J. Cravens, "Electric propulsion study (AL-TR-89-040)," Air Force Astronautics Lab, Edwards AFB, CA, USA, 1990.

[3] A. A. Martins and M. J. Pinheiro, "Modeling of an EHD corona flow in nitrogen gas using an asymmetric capacitor for propulsion," J. Electrostatics, Vol. 69, pp. 133-138, 2011.

[4] H.-C. Wang, N. E. Jewell-Larsen, and A. V. Mamishev, "Thermal management of microelectronics with electrostatic fluid accelerators," Appl. Thermal Eng., Vol. 51, pp. 190-211, 2013.

[5] H. J. Schmid, S. Stolz, and H. Buggisch, "On the modelling of the electro-hydrodynamic flow field in electrostatic precipitators," Flow, Turbulence and Combustion, Vol. 68, pp. 63-89, 2002.

[6] R.-T. Huang, W.-J. Sheu, and C.-C. Wang, "Heat transfer enhancement by needle-arrayed electrodes – An EHD integrated cooling system," Energy Conversion and Management, Vol. 50, pp. 1789-1796, 2009.

[7] S. Lynikiene, "Carrot seed preparation in a corona discharge field," CIGR J. Scientific Research and Development, Vol. 3, 2001.

[8] J. S. E. Townsend, *Electricity in Gases*, Oxford: Clarendon Press, 1915.

[9] R. S. Sigmond, "Simple approximate treatment of unipolar space-charge-dominated coronas: The Warburg law and the saturation current," J. Appl. Phys., Vol. 53, pp. 891-898, Feb. 1982.

[10] R. S. Sigmond, "The unipolar corona space charge flow problem," J. Electrostatics, Vol. 18, pp. 249-272, 1986.

[11] K. Yanallah, F. Pontiga, A. Fernandez-Rueda, A. Castellanos, and A. Belasri, "Ozone generation using negative wire-to-cylinder corona discharge: the influence of anode composition and radius," IEEE Conf. Electr. Insul. Dielectr. Phenomena (CEIDP), pp. 607-610, 2008.
[12] J. C. Matéo-Vélez, P. Degond, F. Rogier, A. Séraudie, and F. Thivet, "Modelling wire-to-wire corona discharge action on aerodynamics and comparison with experiment," J. Phys. D: Appl. Phys., Vol. 41, p. 035205, 2008.
[13] K. S. P. Nikas, A. A. Varonos, and G. C. Bergeles, "Numerical simulation of the flow and the collection mechanisms inside a laboratory scale electrostatic precipitator," J. Electrostatics, Vol. 63, pp. 423-443, 5// 2005.
[14] J.-D. Moon, D.-H. Hwang, J.-S. Jung, J.-G. Kim, and S.-T. Geum, "A sliding discharge-type EHD gas pump utilizing a saw-toothed-plate discharge electrode," IEEE Trans. Dielectr. Electr. Insul., Vol. 17, pp. 742-747, 2010.
[15] N. E. Jewell-Larsen, E. Tran, I. A. Krichtafovitch, and A. V. Mamishev, "Design and optimization of electrostatic fluid accelerators," IEEE Trans. Dielectr. Electr. Insul., Vol. 13, pp. 191-203, 2006.
[16] M. Tanski, M. Kocik, and J. Mizeraczyk, "Electrohydrodynamic gas pump with both insulated electrodes driven by dielectric barrier discharge," IEEE Trans. Dielectr. Electr. Insul., Vol. 18, pp. 1429-1432, 2011.
[17] A. Jaworek and A. T. Sobczyk, "Electrospraying route to nanotechnology: An overview," J. Electrostatics, Vol. 66, pp. 197-219, 2008.
[18] J.-H. Kim, H.-S. Lee, H.-H. Kim, and A. Ogata, "Electrospray with electrostatic precipitator enhances fine particles collection efficiency," J. Electrostatics, Vol. 68, pp. 305-310, No. 8, 2010.
[19] E. Moreau and G. Touchard, "Enhancing the mechanical efficiency of electric wind in corona discharges," J. Electrostatics, Vol. 66, pp. 39-44, 2008.
[20] M. S. June, J. Kribs, and K. M. Lyons, "Measuring efficiency of positive and negative ionic wind devices for comparison to fans and blowers," J. Electrostatics, Vol. 69, pp. 345-350, 2011.
[21] J. Kuffel, E. Kuffel, and W. Zaengl, *High Voltage Engineering Fundamentals*, Newnes, 2000.
[22] M. Abdel-Salam, *High-Voltage Engineering: Theory and Practice*, Revised and Expanded: CRC Press, 2000.
[23] J. Holtzhausen and W. Vosloo, *High Voltage Engineering Practice and Theory*. Netherlands, 2003.
[24] C. Wadhwa, *High voltage engineering*. India: New Age International, 2007.
[25] E. D. Fylladitakis, A. X. Moronis, and M. Theodoridis, "Analytical Estimation of the Electrostatic Field in Cylinder-plane and Cylinder-cylinder Electrode Configurations," Int'l. J. Electrical and Computer Eng. (IJECE), Vol. 6, pp. 2599-2698, 2016.
[26] S. Cui, "Electrostatic potential in cylindrical dielectric media using the image charge method," Molecular Phys., Vol. 104, pp. 2993-3001, 2006.
[27] H. Wintle, "Unipolar wire-to-plane corona: accuracy of simple approximations," J. Electrostatics, Vol. 28, pp. 149-159, 1992.
[28] R. T. Waters and W. B. Stark, "Characteristics of the stabilized glow discharge in air," J. Phys. D: Appl. Phys., Vol. 8, p. 416-427, 1975.
[29] P. Cooperman, "A theory for space-charge-limited currents with application to electrical precipitation," Amer. Inst. Electr. Engineers, Part I: Trans. Communication and Electronics,, Vol. 79, pp. 47-50, 1960.
[30] V. Mohnen, "Formation, nature, and mobility of ions of atmospheric importance," in *Electrical Processes in Atmospheres*, ed: Springer, pp. 1-17, 1976.
[31] K. Aplin, "Aspirated capacitor measurements of air conductivity and ion mobility spectra," Rev. Scientific Instruments, Vol. 76, p. 104501, 2005.
[32] M. Goldman, A. Goldman, and R. Sigmond, "The corona discharge, its properties and specific uses," Pure and Applied Chem., Vol. 57, pp. 1353-1362, 1985.
[33] F. W. Peek, *Dielectric Phenomena in High Voltage Engineering*, New York: McGraw-Hill Book Company, Inc, 1915.
[34] M. Goldman and R. Sigmond, "Corona and insulation," IEEE Trans. Electr. Insul., Vol. 2, pp. 90-105, 1982.
[35] P. Yan, C. Zheng, G. Xiao, X. Xu, X. Gao, Z. Luo, et al., "Characteristics of negative DC corona discharge in a wire–plate configuration at high temperatures," Separation and Purification Technology, Vol. 139, pp. 5-13, 2015.
[36] G. Yinliang, X. Xiaodong, and C. Baozhi, "Investigation of Current Density Distribution Model for Barb-plate ESP," in *Electrostatic Precipitation*, K. Yan, Ed., ed.: Springer Berlin Heidelberg, 2009, pp. 359-362.
[37] K. J. McLean and I. A. Ansari, "Calculation of the rod-plane voltage/current characteristics using the saturated current density equation and Warburg's law," IEE Proc. A, Physical Sci., Measurement and Instrumentation, Management and Education - Reviews, Vol. 134, pp. 784-788, 1987.

Emmanouil D. Fylladitakis received a B.Sc. degree in electrical energy engineering from the Technological Educational Institute (TEI) of Athens, Athens, Greece, in 2010, an M.Sc. degree in energy with distinction from the Heriot-Watt University, Edinburgh, Scotland, in 2012, where he received a prize for outstanding merit, and a Ph.D. degree from the Electronics and Computer Engineering department of the Brunel University London, U.K, in 2016. His research interests include the study of corona discharges, electrohydrodynamic effects, renewable energy systems, energy conservation in buildings, engineering education and distance learning systems. He currently is an external research associate at the Technological Educational Institute (TEI) of Athens.

Antonios X. Moronis was born in Athens, Greece, in 1967. He received a diploma in electrical engineering from the Aristotle University of Thessaloniki, Greece, in 1990, and a Ph.D. degree in electrical engineering from the National Technical University of Athens in 1995. From 2001 to 2006 he was Assistant Professor with the Energy Engineering Department of Technological Educational Institute, Athens, Greece. Currently he is an Associate Professor at the same Department and director of the Electrotechnology and Measuring Systems laboratory. He is the author of more than 45 articles in scientific journals and conference proceedings. His research interests include dielectrics and electrical insulation, electrohydrodynamics, high voltage applications, earthing systems in electrical installations, and fault diagnosis and predictive maintenance of electric power system components. Dr. Moronis is a member of the Technical Chamber of Greece.

Michael P. Theodoridis received the B.Sc. degree in energy engineering from the Technological Educational Institute (TEI) of Athens, Athens, Greece, in 2000, the M.Sc. degree in power electronics and drives jointly from the University of Birmingham, Birmingham, U.K., and the University of Nottingham, Nottingham, U.K., in 2002, and the Ph.D. degree in electrical engineering from the University of Birmingham in 2005.

From 2000 to 2001, he was at Olympic Airways, Athens, Greece. From 2005 to 2011, he was with the Department of Energy Technology, TEI of Athens. He is currently with Brunel University London, U.K. His research interests include high-frequency converters, electrical machines and drives, and renewable energy.